Distributed Frequency and Voltage Control for AC Microgrids based on Primal-Dual Gradient Dynamics ⋆

Lukas Kölsch * **Katharina Wieninger** * **Stefan Krebs** *
Sören Hohmann *

* *Institute of Control Systems, Karlsruhe Institute of Technology, Karlsruhe, Germany (e-mail: lukas.koelsch@kit.edu)*

Abstract: With the gradual transformation of power generation towards renewables, distributed energy resources are becoming more and more relevant for grid stabilization. In order to involve all participants in the joint solution of this challenging task, we propose a distributed, model-based and unifying controller for frequency and voltage regulation in AC microgrids, based on steady-state optimal control. It not only unifies frequency and voltage control, but also incorporates the classic hierarchy of primary, secondary and tertiary control layers with each closed-loop equilibrium being a minimizer of a user-defined cost function. By considering the individual voltage limits as additional constraints in the corresponding optimization problem, no superordinate specification of voltage setpoints is required. Since the dynamic model of the microgrid has a port-Hamiltonian structure, stability of the overall system can be assessed using shifted passivity properties. Furthermore, we demonstrate the effectiveness of the controller and its robustness against fluctuations in active and reactive power demand by means of numerical examples.

Keywords: distributed control, optimization-based control, electric power systems, microgrids, frequency regulation, voltage regulation

1. INTRODUCTION

Our current energy system is undergoing a rapid change towards an increasing penetration by renewable energy sources. Large, central, conventional power plants are being successively replaced by distributed energy resources (DERs). If interconnected in an islanded microgrid without any superordinate instance, the individual DERs must provide stability by themselves, which has direct implications for the control strategy: On the one hand, control actions must become increasingly faster due to the lack of rotational inertia. On the other hand, the central superordinate authority that ensures stability is increasingly disappearing which in turn requires the control objective to be achieved jointly and decentrally by all participating resources. According to the IEEE-PES Task Force on Microgrid Stability Definitions, Analysis, and Modeling, *"a microgrid is stable if, after being subjected to a disturbance, all state variables recover to (possibly new) steady-state values which satisfy operational constraints (…), and without the occurrence of involuntary load shedding."* (Farrokhabadi et al. (2020)). In terms of frequency and voltage, this entails achieving a steady state where frequencies at each node are equal and correspond to the nominal frequency and where all of the individual voltage magnitudes remain within certain limits.

Such a complex requirement can be met conveniently using primal-dual gradient dynamics by characterizing the desired equilibrium as an optimizer of a constrained optimization problem. In the existing literature, promising approaches have already been developed to enable frequency (Stegink et al. (2017b); Mallada et al. (2017)) and voltage regulation (Magnússon et al. (2017)) in AC microgrids by this method, see Mohagheghi et al. (2018) and Dörfler et al. (2019) for an extensive survey on current research directions on optimization-based control of future power grids and Simpson-Porco et al. (2016) and Chen and You (2017) for rigorous performance analysis of the primal-dual method with a DC power flow approximation. However, the existing control approaches always pursue only one of the two objectives or implicitly assume that specific voltage setpoints are already provided by a higher level authority.

To meet the above requirements in the original and genuine sense, we present a unifying frequency and voltage controller using primal-dual gradient dynamics in this paper. It allows real-time optimization of the connected DERs as well as conventional generators, with the primary goal of maintaining the nominal frequency and keeping all voltage magnitudes within pre-defined limits while minimizing a user-defined cost function. Our controller is unifying in the sense that the former hierarchical division into primary, secondary and tertiary frequency and voltage control tasks is combined within a single controller and that frequency and voltage stabilization as specified above is maintained simultaneously. In particular, no communication of superordinate set points by a higher-level authority is necessary. The controller design is based on a nonlinear
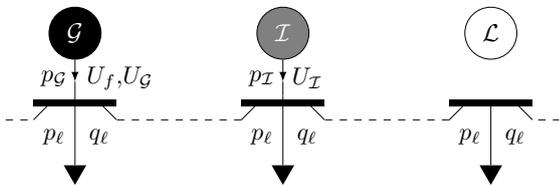

Fig. 1. Schematic illustration of synchronous generator ($\mathcal{G}$), inverter ($\mathcal{I}$), and load nodes ($\mathcal{L}$)

port-Hamiltonian model for AC microgrids (Kölsch et al. (2019b)) and allows for a distributed implementation.

The remainder of the paper is structured as follows. After some notational preliminaries, in section 2, we briefly recall the underlying microgrid model from Kölsch et al. (2019b) and then formalize the requirements for the desired closed-loop equilibrium. In section 3, we derive a price-based controller for frequency and voltage regulation that meets the previously formulated requirements. Moreover, we assess shifted passivity of the subsystems and stability of the overall system. In section 4, we demonstrate the performance of the closed-loop system against input disturbances by means of a 12-node test network and in section 5, we give a brief summary of the main results.

Notation   Vector $\boldsymbol{a} = \mathrm{col}_i\{a_i\} = \mathrm{col}\{a_1, a_2, \ldots\}$ is a column vector of elements a_i, $i = 1, 2, \ldots$ and matrix $\boldsymbol{A} = \mathrm{diag}_i\{a_i\} = \mathrm{diag}\{a_1, a_2, \ldots\}$ is a (block-)diagonal matrix of elements a_i, $i = 1, 2, \ldots$. The $(n \times n)$-identity matrix is denoted by $\boldsymbol{I}_n$ and the all-ones vector is denoted by $\mathbb{1}$. Positive semi-definite matrices are denoted by $\succeq 0$ and positive definite matrices or functions are denoted by $\succ 0$. Equilibrium variables are marked with an asterisk and shifted values with respect to an equilibrium are marked with a tilde, i.e. $\widetilde{\boldsymbol{x}} = \boldsymbol{x} - \boldsymbol{x}^\star$. If lower and upper bounds are specified for a particular quantity x, these are marked with $\underline{x}$ and $\overline{x}$, respectively. For a given $\mu \geq 0$, we define

$$\langle\!\langle x \rangle\!\rangle_\mu^+ := \begin{cases} x, & \mu > 0 \vee x \geq 0 \\ 0, & \text{else} \end{cases}. \quad (1)$$

If $\boldsymbol{x}$ and $\boldsymbol{\mu}$ are vectors of the same size $i \in \mathbb{N}$, then (1) can be applied component-wise, i.e. $\langle\!\langle \boldsymbol{x} \rangle\!\rangle_{\boldsymbol{\mu}}^+ : \mathrm{col}_i\{\langle\!\langle x_i \rangle\!\rangle_{\mu_i}^+\}$.

2. SYSTEM MODEL AND PROBLEM FORMULATION

2.1 Microgrid model

The microgrid is modeled by a directed graph $\mathscr{G}_p = (\mathcal{V}, \mathcal{E}_p)$ with $\mathcal{V} = \mathcal{V}_\mathcal{G} \cup \mathcal{V}_I \cup \mathcal{V}_\mathcal{L}$ being the set of $n_\mathcal{G} = |\mathcal{V}_\mathcal{G}|$ synchronous generator nodes , $n_\mathcal{I} = |\mathcal{V}_I|$ inverter nodes, and $n_\mathcal{L} = |\mathcal{V}_\mathcal{L}|$ load nodes. These three different node types are introduced to model the connection to different microgrid participants, see Fig. 1:

(1) Synchronous generator nodes are connected to synchronous generators of e.g. gas or hydro turbines.
(2) Inverter nodes are connected to power electronics interfaced DERs such as photovoltaic power stations.
(3) Load nodes are connected to consumers with uncontrollable power demand or alternatively to uncontrollable power sources (modeled as negative demands).

Table 1. List of Microgrid Parameters

Symbol	Variable
A_i	positive damping coefficient
B_{ii}	negative of self-susceptance
B_{ij}	negative of susceptance of line (i, j)
G_{ij}	negative of conductance of line (i, j)
L_i	deviation of angular momentum from nominal value $M_i \omega^n$
M_i	moment of inertia
p_i	sending-end active power flow
$p_{g,i}$	active power generation
$p_{\ell,i}$	active power demand
q_i	sending-end reactive power flow
$q_{\ell,i}$	reactive power demand
U_i	magnitude of transient internal voltage
$U_{f,i}$	magnitude of excitation voltage
$X_{d,i} - X'_{d,i}$	d-axis synchronous minus transient reactance
θ_i	bus voltage phase angle
ϑ_{ij}	bus voltage angle difference
Φ	overall transmission losses
$\tau_{U,i}$	open-circuit transient time constant of synchronous machine
ω_i	deviation of bus frequency from nominal value

All nodes may be equipped with a given and uncontrollable active and reactive power demand $\boldsymbol{p}_\ell$ and $\boldsymbol{q}_\ell$ which is modelled as disturbance input. The controlled variables are active power injection $p_\mathcal{G}$ and excitation voltage $\boldsymbol{U}_f$ at generator nodes and active power injection $\boldsymbol{p}_\mathcal{I}$ and AC terminal voltage $\boldsymbol{U}_\mathcal{I}$ at inverter nodes. A list of all microgrid parameters used in the following can be found in Table 1. The inverter interface is assumed to be equipped with an internal matching controller which allows to determine a "virtual" moment of inertia and a "virtual" damping constant for the respective nodes as shown e.g. in Jouini et al. (2016) and Monshizadeh et al. (2017). Furthermore we make the following operating assumptions for the microgrid:

Assumption 1.   a) The grid is a balanced three-phased system and the lines are represented by its one-phase π-equivalent circuits.
   b) The grid is operating around the nominal frequency.
   c) Subtransient dynamics of the synchronous generators is neglected.
   d) The internal matching controller of the inverters has fast dynamics compared to the gradient-based frequency and voltage controller.

The physical interconnection of the nodes is represented by an incidence matrix $\boldsymbol{D}_p \in \mathbb{R}^{n \times m_p}$ with $n = n_\mathcal{G} + n_\mathcal{I} + n_\mathcal{L}$ and $m_p = |\mathcal{E}_p|$. The incidence matrix $\boldsymbol{D}_p$ can be subdivided as $\boldsymbol{D}_p = \mathrm{col}\{\boldsymbol{D}_{p\mathcal{G}}, \boldsymbol{D}_{p\mathcal{I}}, \boldsymbol{D}_{p\mathcal{L}}\}$, where submatrices $\boldsymbol{D}_{p\mathcal{G}}$, $\boldsymbol{D}_{p\mathcal{I}}$, and $\boldsymbol{D}_{p\mathcal{L}}$ correspond to the generator, inverter, and load nodes, respectively. The sending-end active and reactive power flows from node $i \in \mathcal{V}$ can be calculated by the AC power flow equations [Machowski et al. (2012)]

$$p_i = \sum_{j \in \mathcal{N}_i} B_{ij} U_i U_j \sin(\vartheta_{ij}) + G_{ii} U_i^2$$
$$+ \sum_{j \in \mathcal{N}_i} G_{ij} U_i U_j \cos(\vartheta_{ij}), \qquad i \in \mathcal{V}, \quad (2)$$
$$q_i = - \sum_{j \in \mathcal{N}_i} B_{ij} U_i U_j \cos(\vartheta_{ij}) + B_{ii} U_i^2$$

$$+ \sum_{j \in \mathcal{N}_i} G_{ij} U_i U_j \sin(\vartheta_{ij}), \qquad i \in \mathcal{V} \qquad (3)$$

with $\boldsymbol{G}$ and $\boldsymbol{B}$ being the conductance and susceptance matrix, respectively, and $\vartheta_{ij} = \theta_i - \theta_j$ being the voltage angle deviation between two adjacent nodes. $\mathcal{N}_i$ denotes the set of neighbors of i, i.e. $j \in \mathcal{N}_i$ if $(i,j) \in \mathcal{E}_p$ or $(j,i) \in \mathcal{E}_p$.

The dynamics of the individual generator, inverter and load nodes are modeled by the following descriptor system, cf. Kölsch et al. (2019b):

$$\dot{\theta}_i = \omega_i, \qquad i \in \mathcal{V}, \qquad (4)$$

$$\dot{L}_i = -A_i \omega_i + p_{g,i} - p_{\ell,i} - p_i, \qquad i \in \mathcal{V}_\mathcal{G} \cup \mathcal{V}_\mathcal{I}, \quad (5)$$

$$\tau_{d,i} \dot{U}_i = U_{f,i} - U_i - \frac{X_{d,i} - X'_{d,i}}{U_i} \cdot q_i, \quad i \in \mathcal{V}_\mathcal{G}, \quad (6)$$

$$0 = -A_i \omega_i - p_{\ell,i} - p_i, \qquad i \in \mathcal{V}_\mathcal{L}, \qquad (7)$$

$$0 = -q_{\ell,i} - q_i, \qquad i \in \mathcal{V}_\mathcal{L}. \qquad (8)$$

Equation (4) defines the relationship between nodal frequencies and angle deviations, (5) describes the active power exchange between the (possibly virtual) mechanical rotor and the neighboring nodes, (6) describes the transient voltage dynamics of sychronous generator nodes and (7)–(8) describe the active and reactive power conservation at load nodes. To obtain a state space representation, we define the plant state vector $\boldsymbol{x}_p$ as

$$\boldsymbol{x}_p = \text{col}\{\boldsymbol{\vartheta}, \boldsymbol{L}_\mathcal{G}, \boldsymbol{L}_\mathcal{I}, \boldsymbol{U}_\mathcal{G}, \boldsymbol{\omega}_\mathcal{L}, \boldsymbol{U}_\mathcal{L}\}, \qquad (9)$$

where for all $i \in \mathcal{V}$, $j \in \mathcal{V}_\mathcal{G}$, $k \in \mathcal{V}_\mathcal{I}$, $l \in \mathcal{V}_\mathcal{L}$:

$$\boldsymbol{\vartheta} = \text{col}_i\{\vartheta_i\}, \qquad \boldsymbol{L}_\mathcal{G} = \text{col}_j\{L_j\}, \qquad (10)$$

$$\boldsymbol{L}_\mathcal{I} = \text{col}_k\{L_k\}, \qquad \boldsymbol{U}_\mathcal{G} = \text{col}_j\{U_j\}, \qquad (11)$$

$$\boldsymbol{\omega}_\mathcal{L} = \text{col}_l\{\omega_l\}, \qquad \boldsymbol{U}_\mathcal{L} = \text{col}_l\{U_l\}. \qquad (12)$$

With the Hamiltonian

$$H_p(\boldsymbol{x}_p) = \frac{1}{2} \sum_{i \in \mathcal{V}_\mathcal{G}} \left(M_i^{-1} L_i^2 + \frac{U_i^2}{X_{d,i} - X'_{d,i}} \right)$$

$$+ \frac{1}{2} \sum_{i \in \mathcal{V}_\mathcal{I}} M_i^{-1} L_i^2$$

$$- \frac{1}{2} \sum_{i \in \mathcal{V}_\mathcal{G}} B_{ii} U_i^2 - \sum_{(i,j) \in \mathcal{E}} B_{ij} U_i U_j \cos(\vartheta_{ij})$$

$$+ \frac{1}{2} \sum_{i \in \mathcal{V}_\mathcal{L}} \omega_{\mathcal{L},i}^2, \qquad (13)$$

and the co-state $\boldsymbol{z}_p = \nabla H(\boldsymbol{x}_p)$, this allows to set up a port-Hamiltonian representation of (2)–(8) as follows

$$\begin{bmatrix} \dot{\boldsymbol{\vartheta}} \\ \dot{\boldsymbol{L}}_\mathcal{G} \\ \dot{\boldsymbol{L}}_\mathcal{I} \\ \dot{\boldsymbol{U}}_\mathcal{G} \\ \boldsymbol{0} \\ \boldsymbol{0} \end{bmatrix} = \underbrace{\begin{bmatrix} \boldsymbol{0} & \boldsymbol{D}_{p\mathcal{G}}^\top & \boldsymbol{D}_{p\mathcal{I}}^\top & \boldsymbol{0} & \boldsymbol{D}_{p\mathcal{L}}^\top & \boldsymbol{0} \\ -\boldsymbol{D}_{p\mathcal{G}} & \boldsymbol{0} & \boldsymbol{0} & \boldsymbol{0} & \boldsymbol{0} & \boldsymbol{0} \\ -\boldsymbol{D}_{p\mathcal{I}} & \boldsymbol{0} & \boldsymbol{0} & \boldsymbol{0} & \boldsymbol{0} & \boldsymbol{0} \\ \boldsymbol{0} & \boldsymbol{0} & \boldsymbol{0} & \boldsymbol{0} & \boldsymbol{0} & \boldsymbol{0} \\ -\boldsymbol{D}_{p\mathcal{L}} & \boldsymbol{0} & \boldsymbol{0} & \boldsymbol{0} & \boldsymbol{0} & \boldsymbol{0} \\ \boldsymbol{0} & \boldsymbol{0} & \boldsymbol{0} & \boldsymbol{0} & \boldsymbol{0} & \boldsymbol{0} \end{bmatrix}}_{\boldsymbol{J}_p}$$

$$- \underbrace{\begin{bmatrix} \boldsymbol{0} & \boldsymbol{0} & \boldsymbol{0} & \boldsymbol{0} & \boldsymbol{0} & \boldsymbol{0} \\ \boldsymbol{0} & \boldsymbol{A}_\mathcal{G} & \boldsymbol{0} & \boldsymbol{0} & \boldsymbol{0} & \boldsymbol{0} \\ \boldsymbol{0} & \boldsymbol{0} & \boldsymbol{A}_\mathcal{I} & \boldsymbol{0} & \boldsymbol{0} & \boldsymbol{0} \\ \boldsymbol{0} & \boldsymbol{0} & \boldsymbol{0} & \boldsymbol{R}_\mathcal{G} & \boldsymbol{0} & \boldsymbol{0} \\ \boldsymbol{0} & \boldsymbol{0} & \boldsymbol{0} & \boldsymbol{0} & \boldsymbol{A}_\mathcal{L} & \boldsymbol{0} \\ \boldsymbol{0} & \boldsymbol{0} & \boldsymbol{0} & \boldsymbol{0} & \boldsymbol{0} & \widehat{\boldsymbol{U}}_\mathcal{L} \end{bmatrix}}_{\boldsymbol{R}_p} \boldsymbol{z}_p - \cdots$$

$$\cdots - \underbrace{\begin{bmatrix} \boldsymbol{0} \\ \boldsymbol{\varphi}_\mathcal{G} \\ \boldsymbol{\varphi}_\mathcal{I} \\ \boldsymbol{\varrho}_\mathcal{G} \\ \boldsymbol{\varphi}_\mathcal{L} \\ \boldsymbol{\varrho}_\mathcal{L} \end{bmatrix}}_{\boldsymbol{r}_p} + \begin{bmatrix} \boldsymbol{0} & \boldsymbol{0} & \boldsymbol{0} & \boldsymbol{0} & \boldsymbol{0} \\ \boldsymbol{I} & \boldsymbol{0} & \boldsymbol{0} & \boldsymbol{0} & -\widehat{\boldsymbol{I}}_\mathcal{G} \\ \boldsymbol{0} & \boldsymbol{I} & \boldsymbol{0} & \boldsymbol{0} & -\widehat{\boldsymbol{I}}_\mathcal{I} \\ \boldsymbol{0} & \boldsymbol{0} & \hat{\boldsymbol{\tau}}_U & \boldsymbol{0} & \boldsymbol{0} \\ \boldsymbol{0} & \boldsymbol{0} & \boldsymbol{0} & \boldsymbol{0} & -\widehat{\boldsymbol{I}}_\mathcal{L} \\ \boldsymbol{0} & \boldsymbol{0} & \boldsymbol{0} & -\boldsymbol{I} & \boldsymbol{0} \end{bmatrix} \begin{bmatrix} \boldsymbol{p}_\mathcal{G} \\ \boldsymbol{p}_\mathcal{I} \\ \boldsymbol{U}_f \\ \boldsymbol{q}_\ell \\ \boldsymbol{p}_\ell \end{bmatrix}, \quad (14)$$

where

$$\boldsymbol{A}_\mathcal{G} = \text{diag}_i\{A_i\}, \qquad i \in \mathcal{V}_\mathcal{G}, \quad (15)$$

$$\boldsymbol{A}_\mathcal{I} = \text{diag}_i\{A_i\}, \qquad i \in \mathcal{V}_\mathcal{I}, \quad (16)$$

$$\boldsymbol{A}_\mathcal{L} = \text{diag}_i\{A_i\}, \qquad i \in \mathcal{V}_\mathcal{L}, \quad (17)$$

$$\boldsymbol{R}_\mathcal{G} = \text{diag}_i\left\{(X_{di} - X'_{di})/\tau_{U,i}\right\}, \qquad i \in \mathcal{V}_\mathcal{G}, \quad (18)$$

$$\widehat{\boldsymbol{U}}_\mathcal{L} = \text{diag}_i\{U_i\}, \qquad i \in \mathcal{V}_\mathcal{L}, \quad (19)$$

$$\boldsymbol{\varphi}_\mathcal{G} = \text{col}_i\{G_{ii}U_i^2 + \sum_{j \in \mathcal{N}_i} G_{ij}U_iU_j\cos(\vartheta_{ij})\}, i \in \mathcal{V}_\mathcal{G}, \quad (20)$$

$$\boldsymbol{\varphi}_\mathcal{I} = \text{col}_i\{G_{ii}U_i^2 + \sum_{j \in \mathcal{N}_i} G_{ij}U_iU_j\cos(\vartheta_{ij})\}, i \in \mathcal{V}_\mathcal{I}, \quad (21)$$

$$\boldsymbol{\varphi}_\mathcal{L} = \text{col}_i\{G_{ii}U_i^2 + \sum_{j \in \mathcal{N}_i} G_{ij}U_iU_j\cos(\vartheta_{ij})\}, i \in \mathcal{V}_\mathcal{L}, \quad (22)$$

$$\boldsymbol{\varrho}_\mathcal{G} = \text{col}_i\{R_{g,i} \sum_{j \in \mathcal{N}_i} G_{ij}U_iU_j\sin(\vartheta_{ij})\}, \qquad i \in \mathcal{V}_\mathcal{G}, \quad (23)$$

$$\boldsymbol{\varrho}_\mathcal{L} = \text{col}_i\{\sum_{j \in \mathcal{N}_i} G_{ij}U_iU_j\sin(\vartheta_{ij})\}, \qquad i \in \mathcal{V}_\mathcal{L}, \quad (24)$$

$$\hat{\boldsymbol{\tau}}_U = \text{diag}_i\{1/\tau_{U,i}\}, \qquad i \in \mathcal{V}_\mathcal{G}, \quad (25)$$

$$\widehat{\boldsymbol{I}}_\mathcal{G} = \begin{bmatrix} \boldsymbol{I}_{n_g \times n_g} & \boldsymbol{0}_{n_g \times n_i} & \boldsymbol{0}_{n_g \times n_\mathcal{L}} \end{bmatrix}, \qquad (26)$$

$$\widehat{\boldsymbol{I}}_\mathcal{I} = \begin{bmatrix} \boldsymbol{0}_{n_i \times n_g} & \boldsymbol{I}_{n_i \times n_i} & \boldsymbol{0}_{n_i \times n_\mathcal{L}} \end{bmatrix}, \qquad (27)$$

$$\widehat{\boldsymbol{I}}_\mathcal{L} = \begin{bmatrix} \boldsymbol{0}_{n_\mathcal{L} \times n_g} & \boldsymbol{0}_{n_\mathcal{L} \times n_i} & \boldsymbol{I}_{n_\mathcal{L} \times n_\mathcal{L}} \end{bmatrix}. \qquad (28)$$

The input vector in (14) is composed of the control input $\boldsymbol{u}_p = \text{col}\{\boldsymbol{p}_\mathcal{G}, \boldsymbol{p}_\mathcal{I}, \boldsymbol{U}_f\}$ and the disturbance input $\boldsymbol{d} = \text{col}\{\boldsymbol{q}_\ell, \boldsymbol{p}_\ell\}$.

2.2 Formalization of Control Objective

The specification for zero deviation from nominal frequency ω^n and limitation of voltage magnitudes can be formalized by the following optimization problem:

$$\min_{\boldsymbol{p}_\mathcal{G}, \boldsymbol{p}_\mathcal{I}, \boldsymbol{U}_f} C(\boldsymbol{p}_\mathcal{G}, \boldsymbol{p}_\mathcal{I}) \qquad \text{(OP)}$$

$$\text{subject to} \quad \Phi = \sum_{i \in \mathcal{V}_\mathcal{G}} p_{\mathcal{G},i} + \sum_{i \in \mathcal{V}_\mathcal{I}} p_{\mathcal{I},i} - \sum_{i \in \mathcal{V}} p_{\ell,i}, \quad (29a)$$

$$\underline{\boldsymbol{U}}_\mathcal{G} \leq \boldsymbol{U}_\mathcal{G} \leq \overline{\boldsymbol{U}}_\mathcal{G}, \qquad (29b)$$

$$\underline{\boldsymbol{U}}_\mathcal{I} \leq \boldsymbol{U}_\mathcal{I} \leq \overline{\boldsymbol{U}}_\mathcal{I}. \qquad (29c)$$

$C(\boldsymbol{p}_\mathcal{G}, \boldsymbol{p}_\mathcal{I})$ is a user-defined, strictly convex objective function representing e.g. the electricity generation costs and $\Phi = \mathbb{1}^\top \text{col}\{\boldsymbol{\varphi}_\mathcal{G}, \boldsymbol{\varphi}_\mathcal{I}, \boldsymbol{\varphi}_\mathcal{L}\}$ denotes the overall transmission losses. The active power balance constraint (29a) is necessary for zero frequency deviation, see e.g. Trip et al. (2016).

To enable a formulation as a distributed controller in the process of the subsequent steps, an exact reformulation of (OP) is derived where the balance constraint (29a) is replaced by a sparse set of neighbor-to-neighbor balance constraints. Moreover, since $\boldsymbol{U}_f$ is controllable, box constraints on $\boldsymbol{U}_\mathcal{G}$ are replaced by box constraints on $\boldsymbol{U}_f$:

Proposition 1. An exact reformulation of (OP) is given by

$$\min_{\boldsymbol{p}_{\mathcal{G}},\boldsymbol{p}_{\mathcal{I}},\boldsymbol{U}_f,\boldsymbol{\nu}} \quad C(\boldsymbol{p}_{\mathcal{G}},\boldsymbol{p}_{\mathcal{I}}) \tag{OP$^\sharp$}$$

$$\text{subject to} \quad \boldsymbol{D}_c\boldsymbol{\nu} = \widehat{\boldsymbol{I}}_{\mathcal{G}}^\top \boldsymbol{p}_{\mathcal{G}} + \widehat{\boldsymbol{I}}_{\mathcal{I}}^\top \boldsymbol{p}_{\mathcal{I}} - \boldsymbol{p}_\ell - \boldsymbol{\varphi}, \tag{30a}$$

$$\boldsymbol{\Psi}\left(\underline{\boldsymbol{U}}_{\mathcal{G}}\right) \leq \boldsymbol{U}_f \leq \boldsymbol{\Psi}\left(\overline{\boldsymbol{U}}_{\mathcal{G}}\right), \tag{30b}$$

$$\underline{\boldsymbol{U}}_{\mathcal{I}} \leq \boldsymbol{U}_{\mathcal{I}} \leq \overline{\boldsymbol{U}}_{\mathcal{I}}, \tag{30c}$$

where $\boldsymbol{\varphi} = \text{col}\{\boldsymbol{\varphi}_{\mathcal{G}},\boldsymbol{\varphi}_{\mathcal{I}},\boldsymbol{\varphi}_{\mathcal{L}}\}$, $\boldsymbol{D}_c$ is an incidence matrix of a connected communication graph $\mathscr{G}_c = (\mathcal{V},\mathcal{E}_c)$ and $\boldsymbol{\Psi}(\boldsymbol{U}_{\mathcal{G}}) = \text{col}_i\{\Psi_i(U_{\mathcal{G},i})\}$, $i \in \mathcal{V}_{\mathcal{G}}$ with

$$\Psi_i(U_{\mathcal{G},i}) = U_{\mathcal{G},i}\left(1 + G_{ii}\left(X_{d,i} - X'_{d,i}\right)\right)$$
$$+ \sum_{j \in \mathcal{N}_i} U_j\left(G_{ij}\sin(\vartheta_{ij}) - B_{ij}\cos(\vartheta_{ij})\right). \tag{31}$$

Proof. Let $\boldsymbol{x}_p^\diamond$ be an optimizer of (OP) and $\boldsymbol{x}_p^\sharp$ be an optimizer of (OP$^\sharp$).

To prove that $\boldsymbol{x}_p^\diamond$ fulfills (30a), we first recall that for each equilibrium of (14) it holds that $\boldsymbol{\omega} = \boldsymbol{0}$ (cf. Proposition 1 in Kölsch et al. (2019b)). Accordingly, (5) and (7) can be written as

$$\boldsymbol{0} = \widehat{\boldsymbol{I}}_{\mathcal{G}}^\top \boldsymbol{p}_{\mathcal{G}} + \widehat{\boldsymbol{I}}_{\mathcal{I}}^\top \boldsymbol{p}_{\mathcal{I}} - \boldsymbol{p}_\ell - \boldsymbol{p} \tag{32}$$

with $\boldsymbol{p} = \text{col}_i\{p_i\}$, $i \in \mathcal{V}$. Inserting (2) in (32) yields

$$\boldsymbol{0} = \widehat{\boldsymbol{I}}_{\mathcal{G}}^\top \boldsymbol{p}_{\mathcal{G}} + \widehat{\boldsymbol{I}}_{\mathcal{I}}^\top \boldsymbol{p}_{\mathcal{I}} - \boldsymbol{p}_\ell - \boldsymbol{\varphi} - \boldsymbol{\phi} \tag{33}$$

with $\boldsymbol{\phi} = \text{col}_i\{\phi_i\}$, $\phi_i = \sum_{j \in \mathcal{N}_i} B_{ij}U_iU_j\sin(\vartheta_{ij})$. Equation (33) is equivalent to (30a) if and only if there exists a $\boldsymbol{\nu} \in \mathbb{R}^{m_c}$ with $\boldsymbol{D}_c\boldsymbol{\nu} = \boldsymbol{\phi}$. Since $\boldsymbol{D}_c$ is the incidence matrix of a connected graph, $\text{rank}(\boldsymbol{D}_c) = n - 1$ and we can delete e.g. the last row to obtain the reduced system

$$\boldsymbol{D}_c^{\text{red}}\boldsymbol{\nu} = \boldsymbol{\phi}^{\text{red}}, \tag{34}$$

again with $\text{rank}(\boldsymbol{D}_c^{\text{red}}) = n - 1$. Note that (34) is a system of $n - 1$ linear equations and m_c variables. Since $\mathscr{G}_c$ is assumed to be connected, m_c must be greater than or equal to $n - 1$. This implies that (34) is underdetermined and hence there always exists a $\boldsymbol{\nu}$ satisfying (30a).

To proove that $\boldsymbol{x}_p^\sharp$ fulfills (29a), left-multiply (30a) with $\mathbb{1}^\top$ which yields

$$\Phi^\sharp = \sum_{i \in \mathcal{V}_{\mathcal{G}}} p_{\mathcal{G},i}^\sharp + \sum_{i \in \mathcal{V}_{\mathcal{I}}} p_{\mathcal{I},i}^\sharp - \sum_{i \in \mathcal{V}} p_{\ell,i}. \tag{35}$$

This completes the proof of the first equivalence.

To proof equivalence of (29b) and (30b), let $\boldsymbol{x}_p^\star$ be an equilibrium of (14). From the fourth row of (14) it follows that for each $i \in \mathcal{V}_{\mathcal{G}}$

$$0 = U_{f,i}^\star - U_{\mathcal{G},i}^\star - \left(X_{d,i} - X'_{d,i}\right)q_i^\star/U_{\mathcal{G},i}^\star. \tag{36}$$

Inserting (3) in (36) and comparing with (31) yields $U_{f,i}^\star = \Psi_i(U_{\mathcal{G},i}^\star)$. Since $G_{ii} \geq 0$ and $X_{d,i} - X'_{d,i} > 0$, it follows that $\nabla\Psi_i(U_{\mathcal{G},i}) = (1 + G_{ii}(X_{d,i} - X'_{d,i})) > 0$, i.e. $\Psi_i(U_{\mathcal{G},i})$ is a strictly increasing affine map, thus $\boldsymbol{U}_{\mathcal{G}}^\star \leq \overline{\boldsymbol{U}}_{\mathcal{G}} \iff \boldsymbol{\Psi}(\boldsymbol{U}_{\mathcal{G}}^\star) \leq \boldsymbol{\Psi}(\overline{\boldsymbol{U}}_{\mathcal{G}})$ and $\underline{\boldsymbol{U}}_{\mathcal{G}} \leq \boldsymbol{U}_{\mathcal{G}}^\star \iff \boldsymbol{\Psi}(\underline{\boldsymbol{U}}_{\mathcal{G}}) \leq \boldsymbol{\Psi}(\boldsymbol{U}_{\mathcal{G}}^\star)$. This completes the proof of the second equivalence.

To sum up, each $\boldsymbol{x}_p^\diamond$ is feasible for (OP$^\sharp$) and each $\boldsymbol{x}_p^\sharp$ is feasible for (OP), thus (OP) and (OP$^\sharp$) are equivalent. ∎

3. CONTROLLER DESIGN

Now, for optimization problem (OP$^\sharp$), a primal-dual gradient controller [Jokic et al. (2009); Stegink et al. (2017b,a)]

can be applied so that together with (14), a closed-loop equilibrium is achieved which is the solution of (OP$^\sharp$). To shorten the notation, denote the vector of active power generations by $\boldsymbol{p}_g$, i.e. $\boldsymbol{p}_g = \text{col}\{\boldsymbol{p}_{\mathcal{G}},\boldsymbol{p}_{\mathcal{I}}\}$.

3.1 Primal-Dual Gradient Controller

Proposition 2. Suppose that some constraint qualification [Boyd and Vandenberghe (2015)] holds for (OP$^\sharp$). Then each closed-loop equilibrium of (14) together with the distributed primal-dual gradient controller

$$\boldsymbol{\tau}_g\dot{\boldsymbol{p}}_g = -\nabla C(\boldsymbol{p}_g) + \widehat{\boldsymbol{I}}_g\boldsymbol{\lambda} + \boldsymbol{u}_c, \tag{37a}$$

$$\boldsymbol{\tau}_\lambda\dot{\boldsymbol{\lambda}} = \boldsymbol{D}_c\boldsymbol{\nu} - \widehat{\boldsymbol{I}}_g^\top \boldsymbol{p}_g + \boldsymbol{p}_\ell + \boldsymbol{\varphi}, \tag{37b}$$

$$\boldsymbol{\tau}_\nu\dot{\boldsymbol{\nu}} = -\boldsymbol{D}_c^\top\boldsymbol{\lambda}, \tag{37c}$$

$$\boldsymbol{\tau}_{\boldsymbol{\mu}_{\mathcal{G}-}}\dot{\boldsymbol{\mu}}_{\mathcal{G}-} = \langle\!\langle \underline{\boldsymbol{\Psi}}_{\mathcal{G}} - \boldsymbol{U}_f \rangle\!\rangle_{\boldsymbol{\mu}_{\mathcal{G}-}}^+, \tag{38a}$$

$$\boldsymbol{\tau}_{\boldsymbol{\mu}_{\mathcal{G}+}}\dot{\boldsymbol{\mu}}_{\mathcal{G}+} = \langle\!\langle \boldsymbol{U}_f - \overline{\boldsymbol{\Psi}}_{\mathcal{G}} \rangle\!\rangle_{\boldsymbol{\mu}_{\mathcal{G}+}}^+, \tag{38b}$$

$$\boldsymbol{\tau}_{U_{\mathcal{G}}}\dot{\boldsymbol{U}}_f = \boldsymbol{\mu}_{\mathcal{G}-} - \boldsymbol{\mu}_{\mathcal{G}+}, \tag{38c}$$

$$\boldsymbol{\tau}_{\boldsymbol{\mu}_{\mathcal{I}-}}\dot{\boldsymbol{\mu}}_{\mathcal{I}-} = \langle\!\langle \underline{\boldsymbol{U}}_{\mathcal{I}} - \boldsymbol{U}_{\mathcal{I}} \rangle\!\rangle_{\boldsymbol{\mu}_{\mathcal{I}-}}^+, \tag{38d}$$

$$\boldsymbol{\tau}_{\boldsymbol{\mu}_{\mathcal{I}+}}\dot{\boldsymbol{\mu}}_{\mathcal{I}+} = \langle\!\langle \boldsymbol{U}_{\mathcal{I}} - \overline{\boldsymbol{U}}_{\mathcal{I}} \rangle\!\rangle_{\boldsymbol{\mu}_{\mathcal{I}+}}^+, \tag{38e}$$

$$\boldsymbol{\tau}_{U_{\mathcal{I}}}\dot{\boldsymbol{U}}_{\mathcal{I}} = -(\nabla\boldsymbol{\Psi}(\boldsymbol{U}_{\mathcal{I}}))^\top(\boldsymbol{\mu}_{\mathcal{G}-} - \boldsymbol{\mu}_{\mathcal{G}+})$$
$$- (\nabla\boldsymbol{\varphi}(\boldsymbol{U}_{\mathcal{I}}))^\top\boldsymbol{\lambda} + \boldsymbol{\mu}_{\mathcal{I}-} - \boldsymbol{\mu}_{\mathcal{I}+} \tag{38f}$$

with $\boldsymbol{u}_c = -\boldsymbol{\omega}$, $\boldsymbol{\tau} > 0$, $\underline{\boldsymbol{\Psi}}_{\mathcal{G}} = \boldsymbol{\Psi}(\underline{\boldsymbol{U}}_{\mathcal{G}})$, $\overline{\boldsymbol{\Psi}}_{\mathcal{G}} = \boldsymbol{\Psi}(\overline{\boldsymbol{U}}_{\mathcal{G}})$ is an optimizer of (OP$^\sharp$).

Proof. The Lagrangian of (OP$^\sharp$) is

$$\mathscr{L}(\boldsymbol{p}_g,\boldsymbol{U}_{\mathcal{G}},\boldsymbol{U}_{\mathcal{I}},\boldsymbol{\nu},\boldsymbol{\lambda},\boldsymbol{\mu}_{\mathcal{G}-},\boldsymbol{\mu}_{\mathcal{G}+},\boldsymbol{\mu}_{\mathcal{I}-},\boldsymbol{\mu}_{\mathcal{I}+}) =$$
$$C(\boldsymbol{p}_{\mathcal{G}},\boldsymbol{p}_{\mathcal{I}}) + \boldsymbol{\lambda}^\top(\boldsymbol{D}_c\boldsymbol{\nu} - \widehat{\boldsymbol{I}}_g^\top\boldsymbol{p}_g + \boldsymbol{p}_\ell + \boldsymbol{\varphi})$$
$$+ \boldsymbol{\mu}_{\mathcal{G}-}^\top(\underline{\boldsymbol{\Psi}}_{\mathcal{G}} - \boldsymbol{U}_f) + \boldsymbol{\mu}_{\mathcal{G}+}^\top(\boldsymbol{U}_f - \overline{\boldsymbol{\Psi}}_{\mathcal{G}})$$
$$+ \boldsymbol{\mu}_{\mathcal{I}-}^\top(\underline{\boldsymbol{U}}_{\mathcal{I}} - \boldsymbol{U}_{\mathcal{I}}) + \boldsymbol{\mu}_{\mathcal{I}+}^\top(\boldsymbol{U}_{\mathcal{I}} - \underline{\boldsymbol{U}}_{\mathcal{I}}). \tag{39}$$

The Karush-Kuhn-Tucker (KKT) conditions specifying a saddle point of $\mathscr{L}$ can be applied to derive a necessary condition for an optimizer of (OP$^\sharp$):

$$\boldsymbol{0} = \nabla C(\boldsymbol{p}_g^\star) - \boldsymbol{\lambda}^\star, \tag{40}$$

$$\boldsymbol{0} = \boldsymbol{D}_c\boldsymbol{\nu}^\star - \widehat{\boldsymbol{I}}_g^\top\boldsymbol{p}_g^\star + \boldsymbol{p}_\ell + \boldsymbol{\varphi}^\star, \tag{41}$$

$$\boldsymbol{0} = \boldsymbol{D}_c^\top\boldsymbol{\lambda}^\star, \tag{42}$$

$$\boldsymbol{0} = -\boldsymbol{\mu}_{\mathcal{G}-}^\star + \boldsymbol{\mu}_{\mathcal{G}+}^\star, \tag{43}$$

$$\boldsymbol{0} = \boldsymbol{\mu}_{\mathcal{G}-}^{\star\top}(\underline{\boldsymbol{\Psi}}_{\mathcal{G}}^\star - \boldsymbol{U}_f^\star), \tag{44}$$

$$\boldsymbol{0} = \boldsymbol{\mu}_{\mathcal{G}+}^{\star\top}(\boldsymbol{U}_f^\star - \overline{\boldsymbol{\Psi}}_{\mathcal{G}}^\star), \tag{45}$$

$$\boldsymbol{0} \leq \boldsymbol{\mu}_{\mathcal{G}-}^\star, \boldsymbol{\mu}_{\mathcal{G}+}^\star, \tag{46}$$

$$\boldsymbol{0} = (\nabla\boldsymbol{\Psi}(\boldsymbol{U}_{\mathcal{I}}^\star))^\top(\boldsymbol{\mu}_{\mathcal{G}-}^\star - \boldsymbol{\mu}_{\mathcal{G}+}^\star)$$
$$+ (\nabla\boldsymbol{\varphi}(\boldsymbol{U}_{\mathcal{I}}^\star))^\top\boldsymbol{\lambda}^\star - \boldsymbol{\mu}_{\mathcal{I}-}^\star + \boldsymbol{\mu}_{\mathcal{I}+}^\star, \tag{47}$$

$$\boldsymbol{0} = \boldsymbol{\mu}_{\mathcal{I}-}^{\star\top}(\underline{\boldsymbol{U}}_{\mathcal{I}}^\star - \boldsymbol{U}_{\mathcal{I}}^\star), \tag{48}$$

$$\boldsymbol{0} = \boldsymbol{\mu}_{\mathcal{I}+}^{\star\top}(\boldsymbol{U}_{\mathcal{I}}^\star - \underline{\boldsymbol{U}}_{\mathcal{I}}^\star), \tag{49}$$

$$\boldsymbol{0} \leq \boldsymbol{\mu}_{\mathcal{I}-}^\star, \boldsymbol{\mu}_{\mathcal{I}+}^\star. \tag{50}$$

Consequently, applying the gradient method (Arrow et al. (1958)) provides (37a)–(38f). ∎

From (37a)–(38f) it follows that the controller is distributed, since each local controller at node i only depends on local measured values as well as values of neighboring nodes $j \in \mathcal{N}_i$. Furthermore, the controller is discontinuous due to the operator (1). Keeping this in mind, we now

analyze convergence of the closed loop-system towards an equilibrium.

3.2 Analysis of Shifted Passivity and Stability

Let $\boldsymbol{d}^\star = \mathrm{col}\{\boldsymbol{q}_\ell^\star, \boldsymbol{p}_\ell^\star\}$ be a given, constant disturbance input vector. We assume in the following that there exists an equilibrium $\boldsymbol{x}^\star$ satisfying the following regularity condition:

Assumption 2. The Hessian of $H_p(\boldsymbol{x}_p)$ is positive definite at steady state $\boldsymbol{x}_p^\star$.

This assumption can be ensured by satisfying e.g. the (relatively mild) operational condition presented in Proposition 9 of Steginík et al. (2017a) and originally derived in Proposition 1 of De Persis and Monshizadeh (2016).

To investigate the shifted passivity of the closed-loop system with respect to $\boldsymbol{x}^\star$, it is convenient to analyze plant system (14), frequency (37a)–(37c), and voltage controller (38a)–(38f) separately.

Proposition 3. The plant system (14) with output $\boldsymbol{y}_p = \boldsymbol{G}_p^\top \boldsymbol{z}_p$ provides a shifted passivity property with respect to $\boldsymbol{x}_p^\star$ if $\left[\boldsymbol{z}_p - \boldsymbol{z}_p^\star\right]^\top \left[\mathcal{R}(\boldsymbol{x}_p) - \mathcal{R}(\boldsymbol{x}_p^\star)\right] \geq 0$ with $\mathcal{R}(\boldsymbol{x}_p) = \boldsymbol{R}_p \boldsymbol{z}_p + \boldsymbol{r}_p$ holds.

Proof. The plant system provides a shifted passivity property with respect to $\boldsymbol{x}_p^\star$ if the shifted plant Hamiltonian $\widetilde{H}_p(\widetilde{\boldsymbol{x}}_p) := H_p(\boldsymbol{x}_p) - (\widetilde{\boldsymbol{x}}_p)^\top \nabla H_p(\boldsymbol{x}_p^\star) - H_p(\boldsymbol{x}_p^\star)$ with $\widetilde{\boldsymbol{x}}_p = \boldsymbol{x}_p - \boldsymbol{x}_p^\star$ satisfies $\widetilde{H}_p(\widetilde{\boldsymbol{x}}_p) \succ 0$ and

$$\dot{\widetilde{H}}_p(\widetilde{\boldsymbol{x}}_p) \leq \widetilde{\boldsymbol{y}}_p^\top \widetilde{\boldsymbol{u}}_p \qquad (51)$$

with $\boldsymbol{y}_p = \boldsymbol{G}_p^\top \boldsymbol{z}_p$. The positive definiteness condition is satisfied locally due to Assumption 2. To investigate (51), with the same reasoning as in Kölsch et al. (2019b), for constant disturbance input $\boldsymbol{d}^\star$, (14) can be expressed in the form

$$\boldsymbol{E}\dot{\widetilde{\boldsymbol{x}}}_p = \boldsymbol{J}_p \nabla \widetilde{H}_p(\boldsymbol{x}) - \left[\mathcal{R}(\boldsymbol{x}_p) - \mathcal{R}(\boldsymbol{x}_p^\star)\right] + \boldsymbol{G}_p \widetilde{\boldsymbol{u}}_p. \qquad (52)$$

With $\dot{\widetilde{H}}_p(\widetilde{\boldsymbol{x}}_p) = \widetilde{\boldsymbol{z}}_p^\top \boldsymbol{E}\dot{\widetilde{\boldsymbol{x}}}_p$ and bearing in mind that $\boldsymbol{J}_p$ is skew-symmetric, this results in the condition of Proposition 3. $\blacksquare$

Note that for lossless grids $\boldsymbol{r}_p = \boldsymbol{0}$, and hence (3) is always fulfilled due to the fact that $\boldsymbol{R}_p \succeq 0$.

Next, we examine the shifted passivity of the frequency controller (37a)–(37c):

Proposition 4. The frequency controller with input $\boldsymbol{u}_c$ and output $\boldsymbol{y}_{u1} = \boldsymbol{p}_g$ provides a shifted passivity property if

$$(\boldsymbol{p}_g - \boldsymbol{p}_g^\star)^\top (\nabla C(\boldsymbol{p}_g) - \nabla C(\boldsymbol{p}_g^\star)) \geq (\boldsymbol{\lambda} - \boldsymbol{\lambda}^\star)^\top (\boldsymbol{\varphi} - \boldsymbol{\varphi}^\star).$$

Proof. By defining the frequency controller state $\boldsymbol{\xi}_1 = \mathrm{col}\{\boldsymbol{\tau}_g \boldsymbol{p}_g, \boldsymbol{\tau}_\lambda \boldsymbol{\lambda}, \boldsymbol{\tau}_\nu \boldsymbol{\nu}\}$ and the frequency controller Hamiltonian $H_1(\boldsymbol{\xi}_1) = \frac{1}{2}\boldsymbol{x}_c^\top \boldsymbol{\tau}_c^{-1} \boldsymbol{x}_c$ with $\boldsymbol{\tau}_c = \mathrm{diag}\{\boldsymbol{\tau}_g, \boldsymbol{\tau}_\lambda, \boldsymbol{\tau}_\nu\} \succ 0$, (37a)–(37c) can be written in port-Hamiltonian form

$$\dot{\boldsymbol{\xi}}_1 = \boldsymbol{J}_1 \nabla H_1(\boldsymbol{\xi}_1) - \boldsymbol{r}_1 + \boldsymbol{G}_{u1}\boldsymbol{u}_c + \boldsymbol{G}_{d1}\boldsymbol{p}_\ell \qquad (53)$$

$$\boldsymbol{y}_{u1} = \boldsymbol{G}_{u1}^\top \boldsymbol{\zeta}_1 \qquad (54)$$

$$\boldsymbol{y}_{d1} = \boldsymbol{G}_{d1}^\top \boldsymbol{\zeta}_1 \qquad (55)$$

where $\boldsymbol{\zeta}_1 = \nabla H_1(\boldsymbol{\xi}_1) = \mathrm{col}\{\boldsymbol{p}_g, \boldsymbol{\lambda}, \boldsymbol{\nu}\}$ and

$$\boldsymbol{J}_1 = \begin{bmatrix} \boldsymbol{0} & \widehat{\boldsymbol{I}}_g & \boldsymbol{0} \\ -\widehat{\boldsymbol{I}}_g^\top & \boldsymbol{0} & \boldsymbol{D}_c \\ \boldsymbol{0} & -\boldsymbol{D}_c^\top & \boldsymbol{0} \end{bmatrix}, \qquad \boldsymbol{r}_1 = \begin{bmatrix} \nabla C(\boldsymbol{p}_g) \\ -\boldsymbol{\varphi} \\ \boldsymbol{0} \end{bmatrix}, \qquad (56)$$

$$\boldsymbol{G}_{u1} = \begin{bmatrix} \boldsymbol{I} \\ \boldsymbol{0} \\ \boldsymbol{0} \end{bmatrix}, \qquad \boldsymbol{G}_{d1} = \begin{bmatrix} \boldsymbol{0} \\ \boldsymbol{I} \\ \boldsymbol{0} \end{bmatrix}. \qquad (57)$$

With the shifted controller Hamiltonian

$$\widetilde{H}_1(\widetilde{\boldsymbol{\xi}}_1) := H_1(\boldsymbol{\xi}_1) - (\widetilde{\boldsymbol{\xi}}_1)^\top \nabla H_1(\boldsymbol{\xi}_1^\star) - H_1(\boldsymbol{\xi}_1^\star), \qquad (58)$$

the shifted controller co-state $\widetilde{\boldsymbol{\zeta}}_1$ equals

$$\widetilde{\boldsymbol{\zeta}}_1 = \nabla \widetilde{H}_1(\widetilde{\boldsymbol{\xi}}_1) = \nabla H_1(\boldsymbol{\xi}_1) - \nabla H_1(\boldsymbol{\xi}_1^\star) = \boldsymbol{\zeta}_1 - \boldsymbol{\zeta}_1^\star. \qquad (59)$$

Since the disturbance input $\boldsymbol{p}_\ell$ is assumed to be constant, (53) can be expressed in shifted coordinates as follows

$$\dot{\widetilde{\boldsymbol{\xi}}}_1 = \boldsymbol{J}_1 \nabla \widetilde{H}_1(\widetilde{\boldsymbol{\xi}}_1) - [\boldsymbol{r}_1(\boldsymbol{\xi}_1) - \boldsymbol{r}_1(\boldsymbol{\xi}_1^\star)] + \boldsymbol{G}_{u1}\widetilde{\boldsymbol{u}}_c, \qquad (60)$$

$$\widetilde{\boldsymbol{y}}_{u1} = \boldsymbol{G}_{u1}^\top \widetilde{\boldsymbol{\zeta}}_1. \qquad (61)$$

Due to strict convexity of $H_1(\boldsymbol{\xi}_1)$, positive definiteness $\widetilde{H}_1(\boldsymbol{\xi}_1) \succ 0$ is always satisfied. Hence the frequency controller is shifted passive if the time derivative

$$\dot{\widetilde{H}}_p(\widetilde{\boldsymbol{x}}_p) = (\nabla \widetilde{H}_1(\widetilde{\boldsymbol{\xi}}_1))^\top \dot{\widetilde{\boldsymbol{\xi}}}_1$$
$$= \widetilde{\boldsymbol{\zeta}}_1^\top [\boldsymbol{r}_1(\boldsymbol{\xi}_1) - \boldsymbol{r}_1(\boldsymbol{\xi}_1^\star)] + \widetilde{\boldsymbol{\zeta}}_1^\top \boldsymbol{G}_{u1}\widetilde{\boldsymbol{u}}_c \qquad (62)$$

fulfills $\dot{\widetilde{H}}_p(\widetilde{\boldsymbol{x}}_p) \leq \widetilde{\boldsymbol{y}}_{u1}^\top \widetilde{\boldsymbol{u}}_c$. Bearing in mind (54), this leads to $\widetilde{\boldsymbol{\zeta}}_1^\top [\boldsymbol{r}_1(\boldsymbol{\xi}_1) - \boldsymbol{r}_1(\boldsymbol{\xi}_1^\star)] \leq 0$, which is equivalent to the condition of Proposition 4. $\blacksquare$

Note that for lossless grids $\boldsymbol{\varphi} = \boldsymbol{0}$, and hence Proposition 4 is always fulfilled due to the fact that $C(\boldsymbol{p}_g)$ is convex.

Since the interconnection between frequency controller and plant system is power-preserving,

$$\boldsymbol{u}_{c1} = -\boldsymbol{y}_{p1} = -\boldsymbol{G}_{p1}^\top \nabla H_p(\boldsymbol{x}_p) = -\boldsymbol{\omega}_g, \qquad (63)$$

$$\boldsymbol{u}_{p1} = \boldsymbol{y}_{c1} = \boldsymbol{G}_{u1}^\top \nabla H_1(\boldsymbol{\xi}_1) = \boldsymbol{p}_g, \qquad (64)$$

shifted passivity of the subsystems in terms of Propositions 3 and 4 implies shifted passivity of the closed-loop system (14),(37a)–(37c). In fact, the conditions stated in Propositions 3 and 4 are not necessary, since as an excess of passivity in one subsystem can compensate for the lack of passivity in the other subsystem, cf. van der Schaft (2017). Based on the previous conditions we now formulate a stability criterion for the overall system with frequency and voltage controller:

Proposition 5. Assume that the conditions of Propositions 3 and 4 hold. For a constant input $\boldsymbol{d}^\star$, let $(\boldsymbol{x}_p^\star, \boldsymbol{\xi}_1^\star, \boldsymbol{\xi}_2^\star)$ denote an equilibrium of (14),(37a)–(38f) and let

$$(\nabla \widetilde{H}_p(\widetilde{\boldsymbol{U}}_\mathcal{I}))^\top \dot{\widetilde{\boldsymbol{U}}}_\mathcal{I} < \widetilde{\boldsymbol{U}}_\mathcal{I}((\nabla \boldsymbol{\Psi}(\boldsymbol{U}_\mathcal{I}))^\top (\boldsymbol{\mu}_{\mathcal{G}-} - \boldsymbol{\mu}_{\mathcal{G}+})$$
$$- \widetilde{\boldsymbol{U}}_\mathcal{I}((\nabla \boldsymbol{\Psi}(\boldsymbol{U}_\mathcal{I}^\star))^\top (\boldsymbol{\mu}_{\mathcal{G}-}^\star - \boldsymbol{\mu}_{\mathcal{G}+}^\star)$$
$$- \widetilde{\boldsymbol{U}}_\mathcal{I}((\nabla \boldsymbol{\varphi}(\boldsymbol{U}_\mathcal{I}))^\top \boldsymbol{\lambda} - (\nabla \boldsymbol{\varphi}(\boldsymbol{U}_\mathcal{I}^\star))^\top \boldsymbol{\lambda}^\star)$$

hold. Then there exists a neighborhood $\mathcal{B}$ around $(\boldsymbol{x}_p^\star, \boldsymbol{\xi}_1^\star, \boldsymbol{\xi}_2^\star)$ such that if $(\boldsymbol{x}_p, \boldsymbol{\xi}_1, \boldsymbol{\xi}_2) \in \mathcal{B}$, then the state asymptotically converges to $(\boldsymbol{x}_p^\star, \boldsymbol{\xi}_1^\star, \boldsymbol{\xi}_2^\star)$.

Proof. With the voltage controller state $\boldsymbol{\xi}_2 = \mathrm{col}\{\boldsymbol{\tau}_{\boldsymbol{\mu}_{\mathcal{G}-}}\boldsymbol{\mu}_{\mathcal{G}-}, \boldsymbol{\tau}_{\boldsymbol{\mu}_{\mathcal{G}+}}\boldsymbol{\mu}_{\mathcal{G}+}, \boldsymbol{\tau}_{U_\mathcal{G}}\boldsymbol{U}_f, \boldsymbol{\tau}_{\boldsymbol{\mu}_{\mathcal{I}-}}\boldsymbol{\mu}_{\mathcal{I}-}, \boldsymbol{\tau}_{\boldsymbol{\mu}_{\mathcal{I}+}}\boldsymbol{\mu}_{\mathcal{I}+}, \boldsymbol{\tau}_{U_\mathcal{I}}\boldsymbol{U}_\mathcal{I}\}$, let $\boldsymbol{\xi}_2^\star$ denote an equilibrium of (38a)–(38f) and define the Lyapunov function candidate $\widetilde{V}_2(\widetilde{\boldsymbol{\xi}}_2) = \frac{1}{2}\widetilde{\boldsymbol{\xi}}_2^\top \boldsymbol{\tau}_2^{-1} \widetilde{\boldsymbol{\xi}}_2^\top$ where $\boldsymbol{\tau}_2 = \mathrm{diag}\{\boldsymbol{\tau}_{\boldsymbol{\mu}_{\mathcal{G}-}}, \boldsymbol{\tau}_{\boldsymbol{\mu}_{\mathcal{G}+}}, \boldsymbol{\tau}_{U_\mathcal{G}},$

$\boldsymbol{\tau_{\mu_{\mathcal{I}-}}}, \boldsymbol{\tau_{\mu_{\mathcal{I}+}}}, \boldsymbol{\tau_{U_{\mathcal{I}}}}\} \succ 0$ and $\widetilde{\boldsymbol{\xi}}_2^\top = \boldsymbol{\xi}_2 - \boldsymbol{\xi}_2^\star$. This allows to set up an overall Lyapunov function candidate $\widetilde{V}(\widetilde{\boldsymbol{x}}_p, \widetilde{\boldsymbol{\xi}}_1, \widetilde{\boldsymbol{\xi}}_2)$ for the overall closed-loop system as the sum of $\widetilde{H}_p$, $\widetilde{H}_1$, and $\widetilde{V}_2$, i.e. $\widetilde{V}(\widetilde{\boldsymbol{x}}_p, \widetilde{\boldsymbol{\xi}}_1, \widetilde{\boldsymbol{\xi}}_2) = \widetilde{H}_p(\widetilde{\boldsymbol{x}}_p, \widetilde{\boldsymbol{\xi}}_2) + \widetilde{H}_1(\widetilde{\boldsymbol{\xi}}_1) + \widetilde{V}_2(\widetilde{\boldsymbol{\xi}}_2) \succ 0$. In the notation of $\widetilde{V}$ it has been taken into account that $\boldsymbol{U}_{\mathcal{I}}$ is contained in the plant Hamiltonian H_p, see (13). With respect to $\dot{\widetilde{V}}$, we observe that

$$\dot{\widetilde{V}}(\widetilde{\boldsymbol{x}}_p, \widetilde{\boldsymbol{\xi}}_1, \widetilde{\boldsymbol{\xi}}_2) = \dot{\widetilde{H}}_p(\widetilde{\boldsymbol{x}}_p, \widetilde{\boldsymbol{\xi}}_2) + \dot{\widetilde{H}}_1(\widetilde{\boldsymbol{\xi}}_1) + \dot{\widetilde{V}}_2(\widetilde{\boldsymbol{\xi}}_2), \quad (65)$$

where the first summand of (65) equals

$$\begin{aligned}\dot{\widetilde{H}}_p(\widetilde{\boldsymbol{x}}_p, \widetilde{\boldsymbol{\xi}}_2) &= (\nabla \widetilde{H}_p(\widetilde{\boldsymbol{x}}_p))^\top \boldsymbol{J}_p(\nabla \widetilde{H}_p(\widetilde{\boldsymbol{x}}_p)) \\ &\quad - (\nabla \widetilde{H}_p(\widetilde{\boldsymbol{x}}_p))^\top \left[\mathcal{R}(\boldsymbol{x}_p) - \mathcal{R}(\boldsymbol{x}_p^\star)\right] \\ &\quad + (\nabla \widetilde{H}_p(\widetilde{\boldsymbol{\xi}}_2))^\top \dot{\widetilde{\boldsymbol{\xi}}}_2 \quad (66) \\ &= -(\boldsymbol{z}_p - \boldsymbol{z}_p^\star)^\top \left[\mathcal{R}(\boldsymbol{x}_p) - \mathcal{R}(\boldsymbol{x}_p^\star)\right] \\ &\quad + (\nabla \widetilde{H}_p(\widetilde{\boldsymbol{\xi}}_2))^\top \dot{\widetilde{\boldsymbol{\xi}}}_2 \quad (67)\end{aligned}$$

due to skew-symmetry of $\boldsymbol{J}_p$. The second summand of (65) is $\dot{\widetilde{H}}_1(\widetilde{\boldsymbol{\xi}}_1) = -\boldsymbol{p}_g^\top(\nabla C(\boldsymbol{p}_g) - \nabla C(\boldsymbol{p}_g^\star)) + (\boldsymbol{\lambda} - \boldsymbol{\lambda}^\star)^\top(\boldsymbol{\varphi} - \boldsymbol{\varphi}^\star)$. The third summand of (65) equals

$$\begin{aligned}\dot{\widetilde{V}}_2(\widetilde{\boldsymbol{\xi}}_2) &= \widetilde{\boldsymbol{\mu}}_{\mathcal{G}-}^\top \langle\!\langle \underline{\boldsymbol{\Psi}}_{\mathcal{G}} - \boldsymbol{U}_f \rangle\!\rangle_{\boldsymbol{\mu}_{\mathcal{G}-}}^+ + \widetilde{\boldsymbol{\mu}}_{\mathcal{G}+}^\top \langle\!\langle \boldsymbol{U}_f - \overline{\boldsymbol{\Psi}}_{\mathcal{G}} \rangle\!\rangle_{\boldsymbol{\mu}_{\mathcal{G}+}}^+ \\ &\quad + \widetilde{\boldsymbol{U}}_f^\top \widetilde{\boldsymbol{\mu}}_{\mathcal{G}-} - \widetilde{\boldsymbol{U}}_f^\top \widetilde{\boldsymbol{\mu}}_{\mathcal{G}+} \\ &\quad + \widetilde{\boldsymbol{\mu}}_{\mathcal{I}-}^\top \langle\!\langle \underline{\boldsymbol{U}}_{\mathcal{I}} - \boldsymbol{U}_{\mathcal{I}} \rangle\!\rangle_{\boldsymbol{\mu}_{\mathcal{I}-}}^+ + \widetilde{\boldsymbol{\mu}}_{\mathcal{I}+}^\top \langle\!\langle \boldsymbol{U}_{\mathcal{I}} - \overline{\boldsymbol{U}}_{\mathcal{I}} \rangle\!\rangle_{\boldsymbol{\mu}_{\mathcal{I}+}}^+ \\ &\quad + \widetilde{\boldsymbol{U}}_{\mathcal{I}}^\top \widetilde{\boldsymbol{\mu}}_{\mathcal{G}-} - \widetilde{\boldsymbol{U}}_{\mathcal{I}}^\top \widetilde{\boldsymbol{\mu}}_{\mathcal{G}+} \\ &\quad + \widetilde{\boldsymbol{U}}_{\mathcal{I}}^\top (\nabla \boldsymbol{\Psi}(\boldsymbol{U}_{\mathcal{I}}))^\top (\boldsymbol{\mu}_{\mathcal{G}-} - \boldsymbol{\mu}_{\mathcal{G}+}) \\ &\quad - \widetilde{\boldsymbol{U}}_{\mathcal{I}}^\top (\nabla \boldsymbol{\Psi}(\boldsymbol{U}_{\mathcal{I}}^\star))^\top (\boldsymbol{\mu}_{\mathcal{G}-}^\star - \boldsymbol{\mu}_{\mathcal{G}+}^\star) \\ &\quad - \widetilde{\boldsymbol{U}}_{\mathcal{I}}^\top ((\nabla \boldsymbol{\varphi}(\boldsymbol{U}_{\mathcal{I}}))^\top \boldsymbol{\lambda} - (\nabla \boldsymbol{\varphi}(\boldsymbol{U}_{\mathcal{I}}^\star))^\top \boldsymbol{\lambda}^\star). \quad (68)\end{aligned}$$

In Proposition 3 of Stegin.k et al. (2015), it was shown that $\widetilde{\boldsymbol{\mu}}^\top \langle\!\langle \boldsymbol{g} \rangle\!\rangle_{\boldsymbol{\mu}}^+ \leq \widetilde{\boldsymbol{\mu}}^\top \boldsymbol{g}$ and $\widetilde{\boldsymbol{\mu}}^\top \boldsymbol{g}^\star \leq \boldsymbol{0}$ holds for each convex function $\boldsymbol{g} = \operatorname{col}_i\{g_i\}$. Hence $\widetilde{\boldsymbol{\mu}}_{\mathcal{G}-}^\top \langle\!\langle \underline{\boldsymbol{\Psi}}_{\mathcal{G}} - \boldsymbol{U}_f \rangle\!\rangle_{\boldsymbol{\mu}_{\mathcal{G}-}}^+ \leq \widetilde{\boldsymbol{\mu}}_{\mathcal{G}-}^\top (\underline{\boldsymbol{\Psi}}_{\mathcal{G}} - \boldsymbol{U}_f) = \widetilde{\boldsymbol{\mu}}_{\mathcal{G}-}^\top (\underline{\boldsymbol{\Psi}}_{\mathcal{G}} - \boldsymbol{U}_f^\star - \widetilde{\boldsymbol{U}}_f) \leq -\widetilde{\boldsymbol{\mu}}_{\mathcal{G}-}^\top \widetilde{\boldsymbol{U}}_f$. With the same procedure it can be calculated for $\mathcal{G}+$, $\mathcal{I}-$, and $\mathcal{I}+$ that the first four rows of (68) are less than or equal to zero, thus $\dot{\widetilde{V}}_2(\widetilde{\boldsymbol{\xi}}_2) \leq \widetilde{\boldsymbol{U}}_{\mathcal{I}}^\top (\nabla \boldsymbol{\Psi}(\boldsymbol{U}_{\mathcal{I}}))^\top (\boldsymbol{\mu}_{\mathcal{G}-} - \boldsymbol{\mu}_{\mathcal{G}+}) - \widetilde{\boldsymbol{U}}_{\mathcal{I}}^\top (\nabla \boldsymbol{\Psi}(\boldsymbol{U}_{\mathcal{I}}^\star))^\top (\boldsymbol{\mu}_{\mathcal{G}-}^\star - \boldsymbol{\mu}_{\mathcal{G}+}^\star) - \widetilde{\boldsymbol{U}}_{\mathcal{I}}^\top (\nabla \boldsymbol{\varphi}(\boldsymbol{U}_{\mathcal{I}}))^\top \boldsymbol{\lambda} - (\nabla \boldsymbol{\varphi}(\boldsymbol{U}_{\mathcal{I}}^\star))^\top \boldsymbol{\lambda}^\star$. With the assumption from Proposition 3, the first row of (67) is ≤ 0 and with the assumption from Proposition 4 it also holds that $\dot{\widetilde{H}}_1(\widetilde{\boldsymbol{\xi}}_1) \leq 0$. Hence $\dot{\widetilde{V}}(\widetilde{\boldsymbol{x}}_p, \widetilde{\boldsymbol{\xi}}_1, \widetilde{\boldsymbol{\xi}}_2) \leq 0$ is fulfilled if

$$\begin{aligned}(\nabla \widetilde{H}_p(\widetilde{\boldsymbol{\xi}}_2))\dot{\widetilde{\boldsymbol{\xi}}}_2 &< \widetilde{\boldsymbol{U}}_{\mathcal{I}}^\top (\nabla \boldsymbol{\Psi}(\boldsymbol{U}_{\mathcal{I}}))^\top (\boldsymbol{\mu}_{\mathcal{G}-} - \boldsymbol{\mu}_{\mathcal{G}+}) \\ &\quad - \widetilde{\boldsymbol{U}}_{\mathcal{I}}^\top (\nabla \boldsymbol{\Psi}(\boldsymbol{U}_{\mathcal{I}}^\star))^\top (\boldsymbol{\mu}_{\mathcal{G}-}^\star - \boldsymbol{\mu}_{\mathcal{G}+}^\star) \\ &\quad - \widetilde{\boldsymbol{U}}_{\mathcal{I}}^\top (\nabla \boldsymbol{\varphi}(\boldsymbol{U}_{\mathcal{I}}))^\top \boldsymbol{\lambda} - (\nabla \boldsymbol{\varphi}(\boldsymbol{U}_{\mathcal{I}}^\star))^\top \boldsymbol{\lambda}^\star)\end{aligned}$$

holds. With $(\nabla \widetilde{H}_p(\widetilde{\boldsymbol{\xi}}_2))^\top \dot{\widetilde{\boldsymbol{\xi}}}_2 = (\nabla \widetilde{H}_p(\widetilde{\boldsymbol{U}}_{\mathcal{I}}))^\top \dot{\widetilde{\boldsymbol{U}}}_{\mathcal{I}}$, this is equal to the condition of Proposition 5. Since $\widetilde{V} \succ 0$ and $\dot{\widetilde{V}} \leq 0$, the discontinuous closed-loop system (14),(37a)–(38f) fulfils the condition of Lemma 4.3 in Cherukuri et al. (2016). According to (Cherukuri et al., 2016, Theorem 4.5), the omega-limit set of each Carathéodory solution of (14),(37a)–(38f) starting in $\mathcal{B}$ is a singleton, hence $(\boldsymbol{x}_p^\star, \boldsymbol{\xi}_1^\star, \boldsymbol{\xi}_2^\star)$ is locally asymptotically stable. ∎
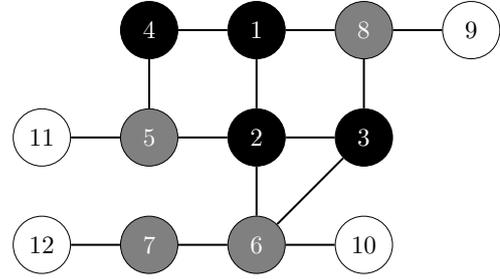

Fig. 2. Network topology of exemplary microgrid.

3.3 Possible Extensions and Variations

The notation as an optimization problem provides numerous possibilities for extending the proposed controller: For example, hard limitations of the active power generation $\boldsymbol{p}_g$ can be incorporated as additional box constraints. Moreover, a simplified controller with a more practical stability criterion can be formulated by assuming lossless transmission lines, i.e. $\boldsymbol{\varphi} = \boldsymbol{0}$, and by exploiting the fact that lower and upper bounds for $\boldsymbol{U}_f$ are relatively insensitive with respect to $\boldsymbol{U}_{\mathcal{I}}$. Simplified' projected bounds $\underline{\boldsymbol{\Psi}}$ and $\overline{\boldsymbol{\Psi}}$ can thus be formulated by replacing all inverter voltage magnitudes $\boldsymbol{U}_{\mathcal{I}}$ in (31) by an estimator $\widehat{\boldsymbol{U}}_{\mathcal{I}}$, e.g. $(\overline{\boldsymbol{U}}_{\mathcal{I}} + \underline{\boldsymbol{U}}_{\mathcal{I}})/2$, to obtain estimators $\widehat{\underline{\boldsymbol{\Psi}}}$ and $\widehat{\overline{\boldsymbol{\Psi}}}$ of the lower and upper bounds which are independent of $\boldsymbol{U}_{\mathcal{I}}$, leading to $\nabla \widehat{\boldsymbol{\Psi}}(\boldsymbol{U}_{\mathcal{I}}) = \boldsymbol{0}$. This gives the following simplified stability criterion:

Corollary 6. Assume that the conditions of Proposition 3 and 4 hold. For a constant input $\boldsymbol{d}^\star$, let $(\boldsymbol{x}_p^\star, \boldsymbol{\xi}_1^\star, \boldsymbol{\xi}_2^\star)$ denote an equilibrium of (14),(37a)–(38f) with zero transmission line losses, i.e. $\boldsymbol{\varphi} = \boldsymbol{0}$, and $\boldsymbol{\Psi} = \widehat{\boldsymbol{\Psi}}$ in (31). If

$$\sum_{i \in \mathcal{V}_{\mathcal{I}}} (\mu_{\mathcal{I}-,i} - \mu_{\mathcal{I}+,i})$$
$$\cdot \Big(\sum_{j \in \mathcal{N}_i} B_{ij} U_j \cos(\vartheta_{ij}) - \sum_{j \in \mathcal{N}_i} B_{ij} U_j^\star \cos(\vartheta_{ij}^\star) \Big) < 0$$

holds, then there exists a neighborhood $\mathcal{B}$ around $(\boldsymbol{x}_p^\star, \boldsymbol{\xi}_1^\star, \boldsymbol{\xi}_2^\star)$ such that if $(\boldsymbol{x}_p, \boldsymbol{\xi}_1, \boldsymbol{\xi}_2) \in \mathcal{B}$, then the state asymptotically converges to $(\boldsymbol{x}_p^\star, \boldsymbol{\xi}_1^\star, \boldsymbol{\xi}_2^\star)$.

Another possible extension is to introduce an additional node type to model controllable active and reactive power input or consumption and to include reactive power limitations in the optimization problem.

4. SIMULATION

We now verify the presented control approach by simulating an exemplary microgrid as presented in Fig. 2 with $n_{\mathcal{G}} = n_{\mathcal{I}} = n_{\mathcal{L}} = 4$.

4.1 Parameterization

The parameter values for all nodes, listed in Tables 2–4, are based on Trip et al. (2016) and Kölsch et al. (2019a), whereby the "virtual" moments of inertia of inverter nodes were selected to be considerably smaller than the corresponding moments of inertia of generator nodes. All values are given in p.u. ($U_{\text{base}} = 20\,\text{kV}$, $S_{\text{base}} = 100\,\text{MVAr}$) except

Table 2. Parameters of Generator Nodes

i	1	2	3	4
A_i	1.6	1.22	1.38	1.42
B_{ii}	-6.0567	-8.014	-6.6755	-4.144
G_{ii}	5.7834	7.86379	5.9209	4.09632
M_i	26.1	19.9	22.45	21.1
$X_{d,i}$	0.15	0.19	0.165	0.1875
$X'_{d,i}$	0.055	0.045	0.055	0.056
$\tau_{U,i}$	6.45	7.68	7.5	6.5

Table 3. Parameters of Inverter Nodes

i	5	6	7	8
A_i	1.4	1.3	1.35	1.45
B_{ii}	-5.6611	-8.1791	-3.6067	-6.1635
G_{ii}	5.77198	7.25506	3.82174	5.74546
M_i	4.4	4.5	5.15	4

Table 4. Parameters of Load Nodes

i	9	10	11	12
A_i	1.45	1.35	1.5	1.7
B_{ii}	-1.716	-2.41244	-1.692	-1.848
G_{ii}	2.05346	1.99349	1.83437	2.02776

Table 5. Parameters of Transmission Lines

(i,j)	B_{ij}	G_{ij}	(i,j)	B_{ij}	G_{ij}
(1,2)	1.905	-1.9167	(3,8)	2.2716	-1.7394
(1,4)	1.976	-2.04	(4,5)	2.168	-2.016
(1,8)	2.176	-1.19178	(5,11)	1.692	-1.7984
(2,3)	2.352	-2.3256	(6,7)	1.7588	-1.7588
(2,5)	1.966	-1.66	(6,10)	2.41244	-1.9544
(2,6)	1.8012	-1.8444	(7,12)	1.848	-1.988
(3,6)	2.052	-1.7396	(8,9)	1.716	-2.0132

$\tau_{U,i}$, which is given in seconds. The transmission line parameters are generated choosing both line resistances R_{ij} and reactances X_{ij} as evenly distributed random variables around $1\,\Omega \pm 10\%$ and can be found in Table 5. In the same fashion, the shunt capacitors at each node are set to $10\,\text{nF} \pm 10\%$. The controller parameters $\boldsymbol{\tau_{\mu_{\mathcal{G}-}}}, \boldsymbol{\tau_{\mu_{\mathcal{G}+}}}$ and $\boldsymbol{\tau_{U_{\mathcal{G}}}}$ are set to 0.01, $\boldsymbol{\tau_{U_{\mathcal{I}}}}$ to 10 and all other controller parameters to 0.1. The cost function is chosen to

$$C(\boldsymbol{p}_g) = \frac{1}{2} \sum_{i \in \mathcal{V}_{\mathcal{G}} \cup V_{\mathcal{I}}} \frac{1}{w_i} \cdot p_{g,i}^2 \qquad (69)$$

with weighting factors $\omega_1 = 1, w_2 = 1.1, w_3 = 1.2$ et cetera. Since $\nabla C(p_i^\star) = \nabla C(p_j^\star)$ at steady state, this specific choice of $C(\boldsymbol{p}_g)$ as a weighted sum of squares leads to *active power sharing*, i.e. a proportional share $p_{g,i}^\star/w_i = p_{g,j}^\star/w_j = \text{const.}$ for all $i,j \in \mathcal{V}_{\mathcal{G}} \cup \mathcal{V}_{\mathcal{I}}$. The voltage limits are set to [0.98 1.02] and the upper bound for active power generation is set to 0.6. We choose $\boldsymbol{D}_c$ to be identical to the plant incidence matrix $\boldsymbol{D}_p$ after it has been pointed out in Kölsch et al. (2019a) that the specific choice of $\boldsymbol{D}_c$ has little influence on the convergence speed to the desired equilibrium. The initial values of disturbance input vector $\boldsymbol{d} = \text{col}\{\boldsymbol{p}_\ell, \boldsymbol{q}_\ell\}$ and state vector $\boldsymbol{x} = \text{col}\{\boldsymbol{x}_p, \boldsymbol{\xi}_1, \boldsymbol{\xi}_2\}$ are chosen such that the closed-loop system starts in synchronous mode with $\boldsymbol{\omega}(t=0) = \boldsymbol{0}$ and such that a number of voltage magnitudes are already close to or at their limits of 0.98 or 1.02. At regular intervals of $200\,\text{s}$, a step of $+0.1\,\text{p.u.}$ active or reactive power demand
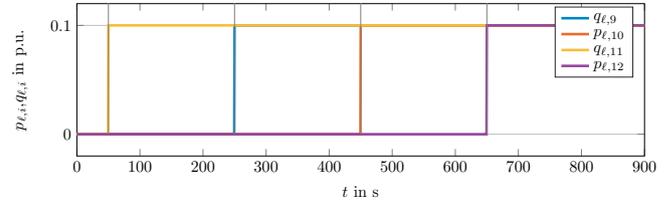

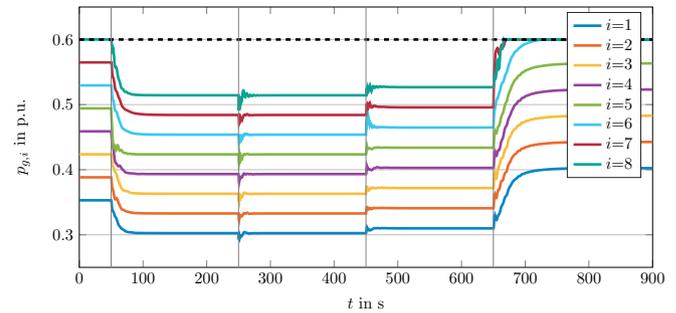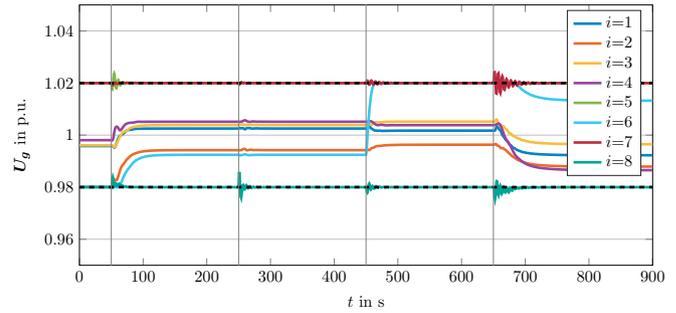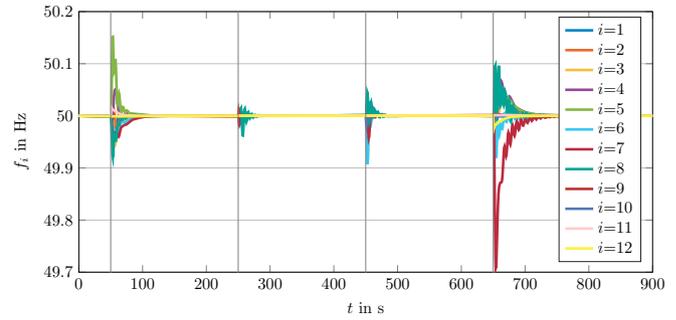Fig. 3. Stepwise increase of active and reactive power demands at load nodes.

Fig. 4. Evolution of frequencies (a), voltage magnitudes (b), and active power generation (c) after step increase

is assigned sequentially at load nodes, see Fig. 3. The simulations are carried out in Wolfram Mathematica 12.0.

4.2 Numerical Results

Fig. 4(a) and 4(b) show the node frequencies and the voltage magnitudes, respectively. It can be seen that in steady state all frequencies are synchronized to $50\,\text{Hz}$ and the voltage limits of 0.98 and 1.02 are kept. The overshoots are around $0.3\,\text{Hz}$ for the node frequencies and $0.005\,\text{p.u.}$ for the voltage amplitudes. Fig. 4(c) shows the corresponding active power generations $\boldsymbol{p}_g$ at generator and inverter nodes. Remarkably, the individual power injections $p_{g,i}$ are equidistant from each other at steady
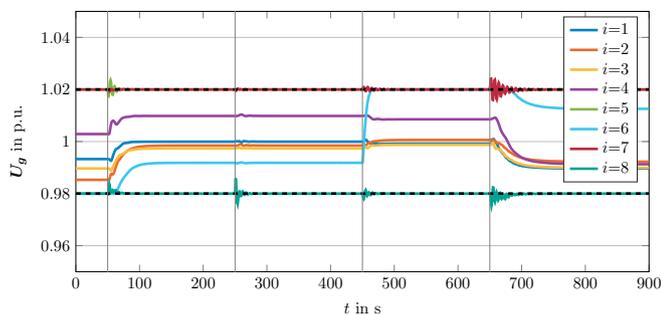
Fig. 5. Evolution of voltage magnitudes if $\boldsymbol{\Psi} = \widehat{\boldsymbol{\Psi}}$.

state, regardless of the total generation, thus active power sharing is given. In addition, it can be stated after the jump at 650 s that the specified maximum limit of 0.6 p.u. for active power generation is not exceeded. Although this limit is reached for nodes 7 and 8, the remaining nodes perform active power sharing without being affected. Fig. 5 shows the voltage magnitudes for the same scenario as above in case the simplified upper and lower limits $\widehat{\overline{\boldsymbol{\Psi}}}$ and $\widehat{\underline{\boldsymbol{\Psi}}}$ are used. Again, overshoots of about 0.005 p.u. can be detected. The progression of voltage magnitudes over time is slightly different, but comparable to Fig. 4(b). In particular, voltage limits are not exceeded at steady state.

5. CONCLUSION

In this paper, we presented a model-based frequency and voltage controller for AC microgrids ensuring optimality with regard to a user-defined cost function. For this purpose, the controller continuously tracks the KKT point of a constrained optimization problem using the gradient method. The underlying nonlinear microgrid model consists of a mixture of conventional synchronous generators, power electronics interfaced sources and uncontrollable loads. The user-defined cost function can be specified in such a way that e.g. active power sharing is achieved. Moreover, the resulting controller equations exhibit a distributed neighbor-to-neighbor communication structure.

REFERENCES

Arrow, K.J., Hurwicz, L., and Uzawa, H. (1958). *Studies in linear and non-linear programming*. Stanford Univ. Press.

Boyd, S.P. and Vandenberghe, L. (2015). *Convex optimization*. Cambridge Univ. Press, Cambridge, 18. edition.

Chen, L. and You, S. (2017). Reverse and forward engineering of frequency control in power networks. *IEEE Trans. Autom. Control*, 62(9), 4631–4638.

Cherukuri, A., Mallada, E., and Cortés, J. (2016). Asymptotic convergence of constrained primal–dual dynamics. *Systems & Control Letters*, 87, 10 – 15.

De Persis, C. and Monshizadeh, N. (2016). A modular design of incremental lyapunov functions for microgrid control with power sharing. In *Proc. European Control Conference*, 1501–1506. IEEE, Piscataway, NJ.

Dörfler, F., Bolognani, S., Simpson-Porco, J.W., and Grammatico, S. (2019). Distributed control and optimization for autonomous power grids. *Proc. European Control Conference*, 2436–2453.

Farrokhabadi, M., Cañizares, C.A., Simpson-Porco, J.W., Nasr, E., Fan, L., Mendoza-Araya, P.A., Tonkoski, R., Tamrakar, U., Hatziargyriou, N., Lagos, D., Wies, R.W., Paolone, M., Liserre, M., Meegahapola, L., Kabalan, M., Hajimiragha, A.H., Peralta, D., Elizondo, M.A., Schneider, K.P., Tuffner, F.K., and Reilly, J. (2020). Microgrid stability definitions, analysis, and examples. *IEEE Trans. Power Systems*, 35(1), 13–29.

Jokic, A., Lazar, M., and van den Bosch, P.P.J. (2009). On constrained steady-state regulation: Dynamic kkt controllers. *IEEE Trans. Autom. Control*, 54(9), 2250–2254.

Jouini, T., Arghir, C., and Dörfler, F. (2016). Grid-friendly matching of synchronous machines by tapping into the dc storage. *IFAC-PapersOnLine*, 49(22), 192–197.

Kölsch, L., Bhatt, K., Krebs, S., and Hohmann, S. (2019a). Steady-state optimal frequency control for lossy power grids with distributed communication. In *Proc. IEEE Conf. Electr., Control & Instrumentation Engineering*.

Kölsch, L., Dupuis, M., Bhatt, K., Krebs, S., and Hohmann, S. (2019b). Distributed frequency regulation for heterogeneous microgrids via steady state optimal control. In *IEEE Green Technologies Conference*. To appear. Preprint available at https://arxiv.org/abs/1910.03115.

Machowski, J., Bialek, J.W., and Bumby, J.R. (2012). *Power system dynamics: Stability and control*. Wiley.

Magnússon, S., Fischione, C., and Li, N. (2017). Voltage control using limited communication. *IFAC-PapersOnLine*, 50(1), 1–6.

Mallada, E., Zhao, C., and Low, S. (2017). Optimal load-side control for frequency regulation in smart grids. *IEEE Trans. Autom. Control*, 62(12), 6294–6309.

Mohagheghi, E., Alramlawi, M., Gabash, A., and Li, P. (2018). A survey of real-time optimal power flow. *Energies*, 11(11), 3142.

Monshizadeh, P., De Persis, C., Stegink, T., Monshizadeh, N., and van der Schaft, A.J. (2017). Stability and frequency regulation of inverters with capacitive inertia. In *Proc. IEEE Conf. Decision Control*, 5696–5701.

Simpson-Porco, J.W., Poolla, B.K., Monshizadeh, N., and Dörfler, F. (2016). Quadratic performance of primal-dual methods with application to secondary frequency control of power systems. In *Proc. IEEE Conf. Decision Control*, 1840–1845.

Stegink, T.W., Persis, C.D., and van der Schaft, A.J. (2017a). Stabilization of structure-preserving power networks with market dynamics. *IFAC-PapersOnLine*, 50, 6737–6742.

Stegink, T., De Persis, C., and van der Schaft, A.J. (2015). Port-hamiltonian formulation of the gradient method applied to smart grids. *IFAC-PapersOnLine*, 48(13), 13–18.

Stegink, T., De Persis, C., and van der Schaft, A.J. (2017b). A unifying energy-based approach to stability of power grids with market dynamics. *IEEE Trans. Autom. Control*, 62(6), 2612–2622.

Trip, S., Bürger, M., and De Persis, C. (2016). An internal model approach to (optimal) frequency regulation in power grids with time-varying voltages. *Automatica*, 64, 240–253.

van der Schaft, A.J. (2017). *L2-Gain and Passivity Techniques in Nonlinear Control*. Springer, Cham.